Dissociation of multicharged CO molecular ions produced in collisions with 97-MeV Ar^{14+}: Total-kinetic-energy distributions

G. Sampoll, R. L. Watson, O. Heber,* V. Horvat,† K. Wohrer,‡ and M. Chabot‡
Cyclotron Institute and Department of Chemistry, Texas A&M University, College Station, Texas 77843
(Received 14 October 1991)

Transient molecular ions of CO^{q+} (where $q=2$–7) were produced in single collisions of 97-MeV Ar^{14+} projectiles with neutral CO molecules. The resulting dissociation products were identified by coincidence time-of-flight spectroscopy in which the time of flight of the first ion to reach the detector and the time difference between the first ion and its partner were recorded event by event. An iterative matrix-transformation procedure was employed to convert the time-difference spectra for the prominent dissociation channels into total-kinetic-energy distributions. Analysis of the total-kinetic-energy distributions and comparisons with the available data for CO^{2+} and CO^{3+} from synchrotron radiation experiments led to the conclusion that ionization by Ar-ion impact populates states having considerably higher excitation energies than those accessed by photoionization.

PACS number(s): 34.50.−s, 35.80.+s, 34.90.+q

I. INTRODUCTION

Many investigations of the dissociative ionization of CO by photons and electrons have been performed in the past. Such studies have provided much information concerning the electronic states of singly charged CO molecular ions. Much less is known about doubly charged CO molecular ions and dissociation products from triply charged CO molecular ions have only been observed in a few experiments [1,2]. The appearance energy for CO^{2+} was initially measured by Dorman and Morrison [3]. Subsequent studies have characterized both the long-lived and the fast-dissociation channels of this molecular ion [4–11].

Recently, the spectroscopy and dynamics of CO^{2+} have been studied by Lablanquie *et al.* [2] using photoionization with 35–150-eV synchrotron radiation, an ion-ion coincidence technique, and H^+ double charge transfer. This investigation identified the CO^{2+} states associated with several of the observed dissociation channels, established the energy threshold for $C^+ + O^+$ ion production via autoionization of highly excited CO^+ states, and reported on the appearance energy and the ion-pair total kinetic energies for the dissociation of CO^{3+} into $C^{2+} + O^+$.

Fast, highly charged ions have been shown to be extremely effective at removing electrons from neutral atomic [12] and molecular collision partners [13–15]. Charge states as high as 8+ in Ne and as high as 11+ in Ar are produced in collisions with 1-MeV/amu Ar^{13+} ions [14]. It follows, therefore, that beams of highly charged heavy ions, available from modern particle accelerators, provide a means for extending the investigation of dissociative ionization up to very-high-charge states.

An extensive survey of the fragmentation patterns of molecular gases produced in collisions of 1-MeV/amu Ar^{13+} was previously carried out by Maurer [16]. In this work, a wide assortment of atomic and molecular ions produced in collisions with simple diatomic (N_2, O_2, CO, and NO), triatiomic (CO_2, N_2O, NO_2, and SO_2), and polyatomic (C_2F_6, $C_2H_4F_2$, and SF_6) molecules were identified through their time-of-flight (TOF) spectra. The information obtained in this study concerning dissociation pathways and dissociation-product kinetic energies was greatly restricted by the fact that only one dissociation-product ion at a time was detected. Subsequently, ion-ion coincidence techniques were adapted to the investigation of multicharged molecular ions produced in fast ion-molecule collisions [17].

In the present work, transient CO^{q+} (where $q=2$–7) molecular ions were produced in collisions with 97-MeV Ar^{14+} ions and the resulting dissociation products identified by coincidence TOF spectroscopy. The differences in the times of flight of the two ions formed in these binary dissociation events were used to deduce the total-kinetic-energy distributions for various charge division pathways. This paper presents a detailed description of the methods used to deduce the total-kinetic-energy distributions of the dissociation products. A forthcoming publication [18] will discuss the dissociation fractions and branching ratios for the various observed dissociation pathways.

II. EXPERIMENTAL METHODS

A beam of 97-MeV Ar^{4+} ions was extracted from the Texas A&M K500 superconducting cyclotron and directed through a stripper foil of 180-$\mu g/cm^2$ Al. Pertinent features of the beam transport system are shown in Fig. 1. An analyzing magnet was used to select Ar^{14+} ions from the distribution of charge states produced in the stripper foil. These ions were transported downstream and focused on the 1-mm-diam entrance aperture of a differentially pumped gas cell.

A schematic diagram of the gas-cell and detector sys-

tems is shown in the inset of Fig. 1. The Ar ions passed through the gas cell at a rate of about 2000/s and entered a particle detector composed of two microchannel plates mounted in a chevron configuration (MCP 1) located 50 cm behind the 2-mm-diam exit aperture of the gas cell. The gas cell was maintained at a pressure of 1 mTorr by means of a capacitance manometer and an automatic valve. This pressure was high enough to achieve a reasonable coincidence counting rate, but low enough to ensure that double collisions were relatively improbable. Ions produced inside the gas cell by Ar-ion impact were accelerated into the flight tube of a TOF spectrometer by an electric field directed perpendicular to the Ar-ion beam. Upon reaching the end of the flight tube, the ions were detected by another set of (chevron) microchannel plates (MCP 2).

The design of the TOF spectrometer was similar to that described in Ref. [19]. Two acceleration stages formed by a grid at the top of the gas cell ($E1$), a 3-mm-diam collimator at the exit of the gas cell ($E2$), and a grid at the entrance of and electrically connected to the flight tube ($E3$) provided space-focusing [20] capability. By adjusting the voltage on $E2$, flight-time differences caused by the 1 mm diameter of the Ar-ion beam could be minimized. The choice of potentials used on electrodes $E1$, $E2$, and $E3$ was basically dictated by the need to (a) resolve the TOF peaks of highly charged ions (such as C^{3+} and C^{4+}), (b) maximize the TOF differences between dissociation partner ions, and (c) achieve an ion transmission efficiency that was large enough to perform the desired ion pair coincidence measurements. The last requirement works in opposition to the other two since (a) and (b) are satisfied by low ΔV, but (c) is fulfilled by high ΔV. The final operating voltages were chosen by flowing Ar gas through the gas cell and studying the voltage dependence of the Ar^{+} to Ar^{11+} recoil-ion TOF peak widths, separations, and counting rates. The final voltages chosen to give the best compromise between resolution and efficiency were $V_{E1}=1200$ V, $V_{E2}=600$ V, and $V_{E3}=0$ V. An analysis of the Ar^{+} TOF peak under these conditions revealed the total instrumental time resolution at time-to-amplitude converter (TAC) 1 to be $3.4\times10^{-3}(\Delta t/t)$ or 6.5 ns full width at half maximum (FWHM) for a TOF of 2.0 μs.

The objectives of the present work were to identify the charges of both ions arising from individual dissociation events and to estimate the relative yields and amounts of kinetic energy released for each of the prominent charge division pathways. In order to accomplish this, it was necessary to measure both the TOF of the first ion of a given dissociation event to reach MCP 2 and the time difference between the arrival of the first ion and its partner. The technique of measuring the difference in arrival times of two ions at the same detector has been commonly employed in studies of dissociative ionization [21]. In the present experiment, two TAC's were used, as shown in Fig. 2. The signals from MCP 2 were used to start TAC 1 and to both start and stop TAC 2. The signals generated by the projectile ions in MCP 1 were delayed by 4 μs and used to stop TAC 1. The start signal for TAC 2 was delayed ($D1$) to prevent starting and stopping with the same signal. Thus, in a successful coincidence event, the first ion to reach MCP 2 would start both TAC 1 and TAC 2. The MCP 2 signal generated upon the arrival of the partner ion would stop TAC 2, thereby completing the time-difference measurement. In the meantime, the MCP 1 signal, having been delayed by 4 μs, would stop TAC 1, thereby completing the TOF

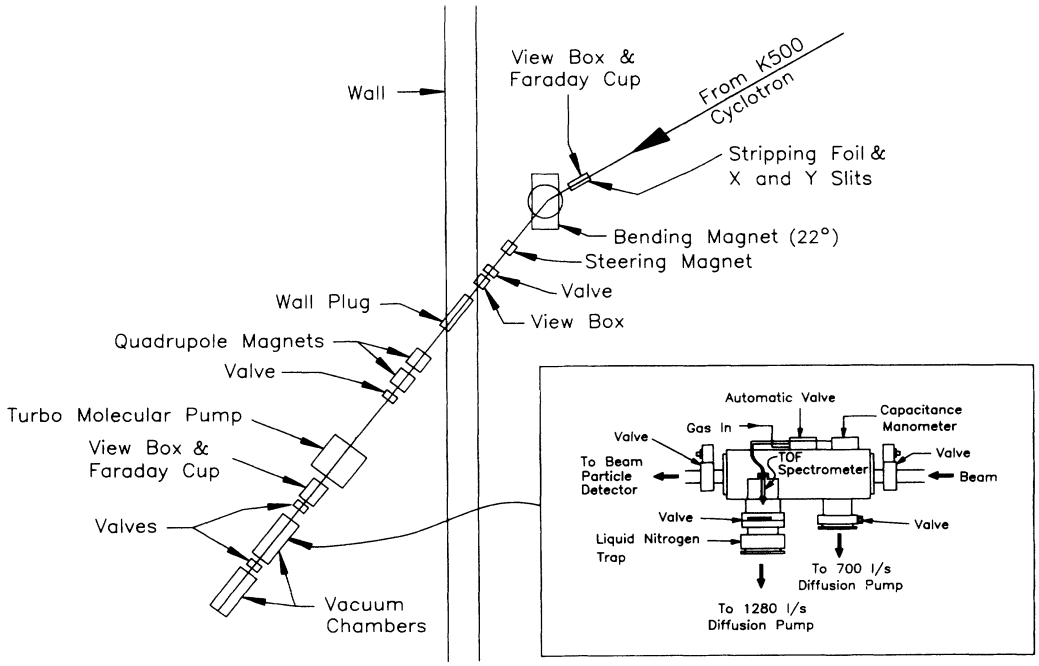

FIG. 1. Schematic diagram of the experimental configuration.

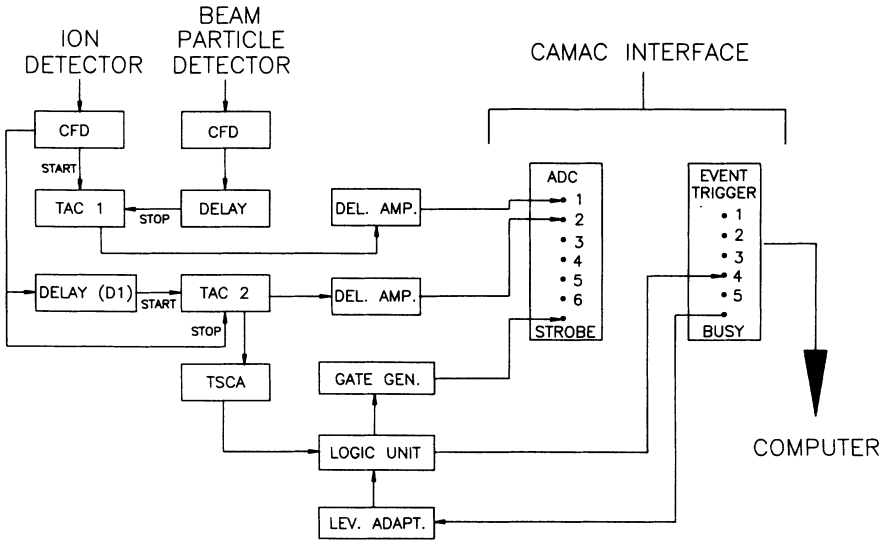

FIG. 2. Schematic diagram of the electronic system. CFD, constant fraction discriminator; TAC, time-to-amplitude converter; TSCA, timing single channel analyzer; ADC, analog-to-digital converter.

measurement of the first ion. The electronic time resolution was 2.4 ns for TAC 1 and 0.73 ns for TAC 2.

The output of each TAC was sent to an analog-to-digital converter (ADC) connected to a microVAX computer via a computer-aided measurement and control (CAMAC) interface and the resulting two-parameter data were recorded on magnetic tape event by event. Event triggers were generated for the computer only when simultaneous outputs were present at both TAC's (i.e., only for coincidence events). A separate multichannel pulse-height analyzer was used to record the singles (i.e. noncoincidence) TOF spectrum from TAC 1.

III. SPECTRAL MEASUREMENTS AND CALIBRATIONS

A. Time-of-flight spectra

A TOF spectrum of Ar, taken for calibration purposes, is shown in Fig. 3(a). Well-defined peaks were observed for all Ar charge states through Ar^{11+}. The H^+ peak originated from residual water vapor in the vacuum system. A plot of the square root of the mass-to-charge ratio versus time of flight, shown in Fig. 3(b), confirmed the linearity of the system.

Calibration of the time scale for TAC 1 was accomplished in two steps. The slope of the time scale was determined from the time spectrum produced by connecting the start and stop outputs of an ORTEC model 462 time calibrator directly to TAC 1. This unit generates pairs of logic signals at precise time intervals corresponding to integer multiples of the time period selected, which in the present application was 160 ns. The accuracy of the time period at this setting is specified by the manufacturer to be ± 8 ps. The intercept of the time calibration was determined by feeding the same pulser signal into both MCP preamplifiers via charge terminators and recording the position of the resulting "zero" time peak in the TAC 1 time spectrum. Since this method did not account for possible differences in the response times of the two MCP's, additional measurements were performed to check this possible source of error. The two MCP's were removed from the TOF system and mounted facing each other. Then a ^{252}Cf source (this nuclide undergoes spontaneous fission) was placed between the two detec-

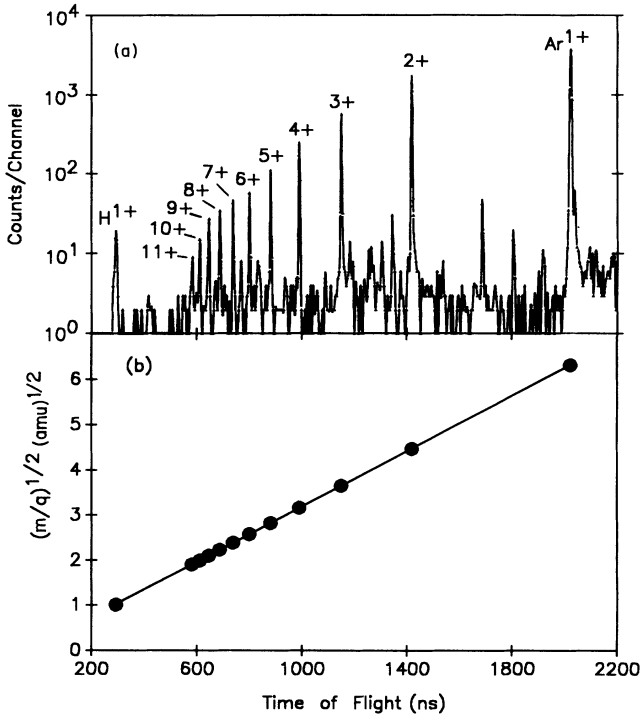

FIG. 3. (a) Time-of-flight spectrum of Ar ions; (b) mass-to-charge ratio calibration for the spectrum in (a).

tors and the time peak resulting from the detection of coincident fission fragments was measured. This time peak was found to deviate from that obtained using the pulser by 5 ns.

The singles and coincidence TOF spectra (TAC 1) measured during the experiment with CO are shown in Figs. 4(a) and 4(b), respectively. The singles spectrum contains all TAC 1 TOF events while the coincidence spectrum contains only those TAC 1 TOF events for which two ions were detected consecutively in MCP 2. Stated more concisely, the coincidence spectrum is the TOF spectrum of first-arrival ions of all detected ion pairs. Identification of each of the TOF peaks was readily accomplished using the $(m/q)^{1/2}$ calibration provided by the Ar TOF spectrum.

In the singles spectrum [Fig. 4(a)], TOF peaks of the molecular ions CO^+ and CO^{2+} are clearly visible along with peaks produced by various C and O dissociation-product ions. It is evident that the dissociation-product ions have considerable amounts of kinetic energy since their peaks are much broader than those of the molecular ions. This kinetic energy must originate from the dissociation process since it has been found in previous studies that very little kinetic energy is transferred from the projectile during the collision [22,23].

Comparing the coincidence spectrum [Fig. 4(b)] with the singles spectrum reveals a number of structural differences. The most striking changes imposed by the coincidence requirement are the large reductions in the relative intensities of the CO^+, O^+, and CO^{2+} peaks. In point of fact, the coincidence requirement should have eliminated these peaks altogether since, in the case of the molecular ions, no ion pairs are produced, and in the case of O^+, all possible C partner ions have shorter flight times and therefore should arrive at MCP 2 before O^+. The majority of the O^+ peak and part of the CO^{2+} peak results from double collisions in which a CO^+ ion is produced also by the same projectile as it traverses the gas cell. The mechanism responsible for the CO^+ peak and part of the CO^{2+} peak is not fully understood. This question will be discussed further in Sec. II B.

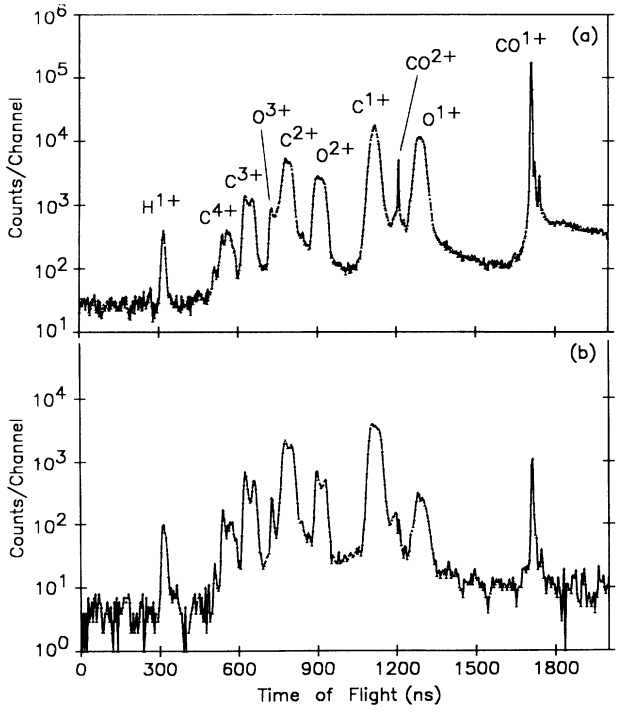

FIG. 4. (a) Noncoincidence and (b) coincidence time-of-flight spectra of ions produced in 97-MeV Ar^{14+} collisions with CO.

Most of the C and O dissociation-product peaks in the coincidence spectrum display a double-peaked structure. This is a consequence of the restrictions placed on the orientation of the intermolecular axis relative to the electric field by the collimator at the exit of the gas cell. Depending on the magnitude of the kinetic energy released in a dissociation event, only an ion pair having initial velocity vectors within a restricted range of angles relative to the field axis would pass through the collimator. Hence, for example, in the dissociation of CO^{5+} to give C^{3+} and O^{2+}, the TOF distribution for C^{3+} ions initially traveling in the upward direction (i.e., away from MCP 2) was sufficiently restricted that it is partially resolved from the TOF distribution for C^{3+} ions initially traveling in the downward direction. Actually each TOF peak contains several TOF distributions with splittings corresponding to rather different kinetic energies. As a case in point, it is noted that the C^{3+} peak contains contributions from C^{3+} ions formed in the dissociation process mentioned above as well as from C^{3+} ions formed in the dissociation processes $CO^{6+} \rightarrow C^{3+} + O^{3+}$ and $CO^{4+} \rightarrow C^{3+} + O^{+}$. In all of these cases, the C^{3+} ion would be the first ion to reach MCP 2. On the other hand, the coincidence requirement excludes contributions to the C^{3+} peak from dissociation processes which produce O ions with charges higher than 4+ (such as $CO^{8+} \rightarrow C^{3+} + O^{5+}$) because the higher charged O ion would arrive at MCP 2 before the C^{3+} ion.

B. Time-difference spectra

The slope of the time scale for TAC 2 was determined using the ORTEC time calibrator, as described for TAC 1 in Sec. II A. The intercept was measured by sending a pulser signal through the preamplifier for MCP 2 and interchanging the start and stop inputs to TAC 2. The position of the time peak produced by TAC 2, under these conditions, corresponded to a time difference exactly equal to the delay $D1$ preceding TAC 2 (see Fig. 2). This delay was set to the minimum value that would produce a TAC 2 output, which turned out to be 17 ns as measured using a fast oscilloscope. Under the conditions of the experiment, the delay $D1$ preceded the start input to TAC 2, and therefore the minimum measurable ion-pair flight time difference was 34 ns.

The total time-difference spectrum (TAC 2) produced in the dissociation of CO^{q+} molecular ions is presented in Fig. 5. This spectrum contains the superimposed distributions of time differences between all detected ion pairs. By placing a window around each (TAC 1) TOF peak accumulated on tape in ADC 1 and sorting out the corresponding (TAC 2) time-difference events accumulat-

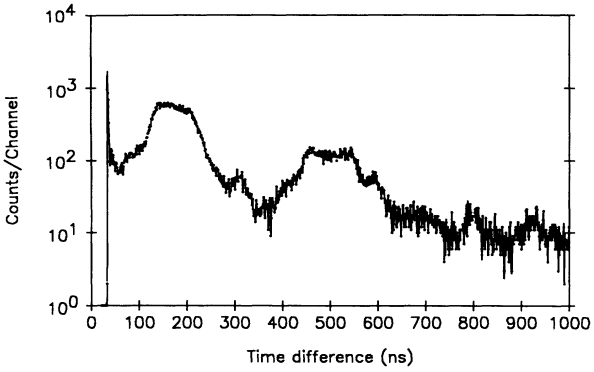

FIG. 5. Total time-difference spectrum for C+O ion pairs from the dissociation of multicharged CO molecular ions.

ed in ADC 2, time-difference spectra for the various ion pairs were separated according to the charge of the first-arrival ion of each pair to arrive at MCP 2. The time-difference spectra for first-arrival C-ion charge states 1+ to 4+ are shown in Fig. 6 and those for first-arrival O-ion charge states 1+ to 3+ are shown in Fig. 7. The data in these two figures have been smoothed using a nine-point averaging procedure. Structural features in these spectra are labeled with the first-arrival ion followed by its dissociation partner (separated by a plus sign). Labels contained in parentheses indicate structural features caused by double-collision events.

Identification of the various ion pairs in Figs. 6 and 7 was easily accomplished by simply matching flight-time differences between the peaks appearing in the singles TOF spectrum [Fig. 4(a)] with the centroid positions of the structural features in the time-difference spectra. For example, the average differences in flight times for C^+ ions and O^+ ions, and for C^+ ions and CO^+ ions are found from Fig. 4(a) to be approximately 170 and 590 ns,

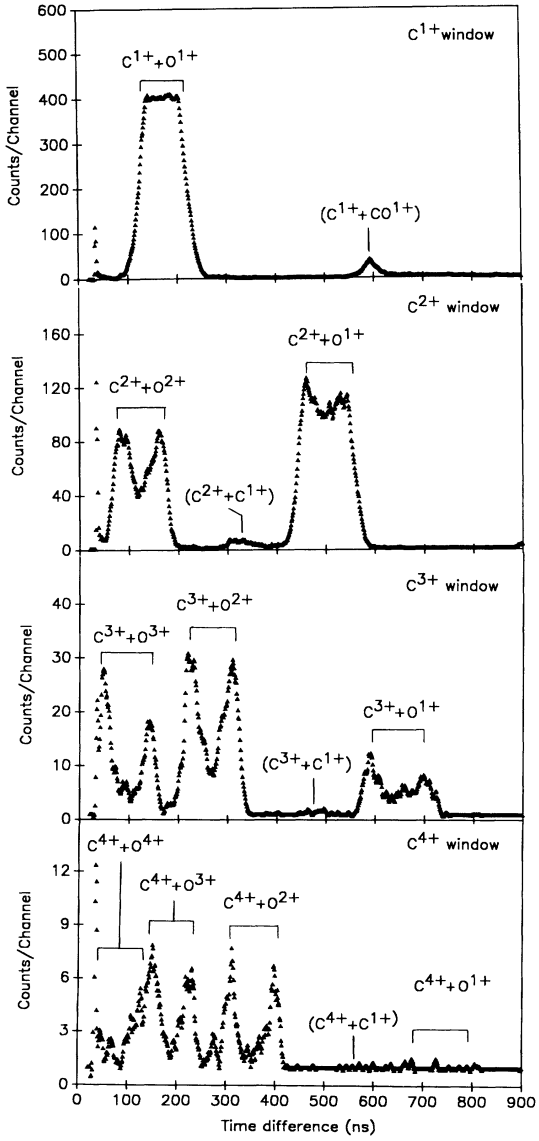

FIG. 6. Sorted time-difference spectra for C^+ through C^{4+} windows.

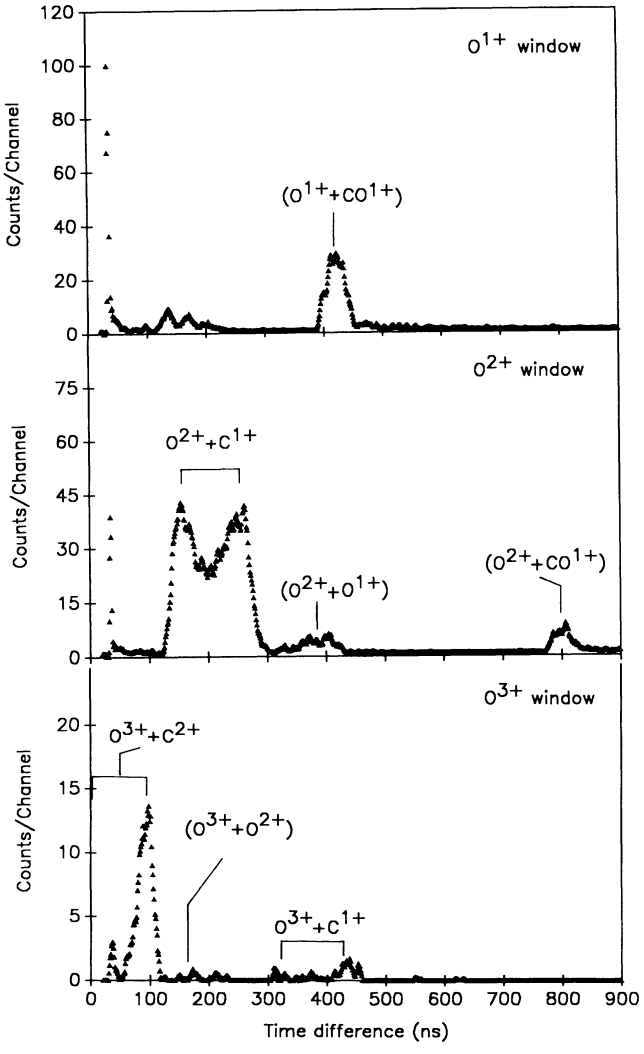

FIG. 7. Sorted time-difference spectra for O^+ through O^{3+} windows.

respectively. These time differences closely correspond to the centroids of the two time-difference distributions appearing in the top segment (C^+ window) of Fig. 6.

The width and shape of a time-difference distribution reflects the distribution of kinetic energy released in the dissociation process. An estimate of the amount of kinetic energy released in a dissociation event may be obtained from the point-charge Coulomb potential between the two product ions at the average internuclear separation for neutral CO (1.1282 Å). This estimation procedure assumes that the dissociative state is formed in a vertical transition during the ionizing collision and it neglects effects associated with the overlap of the electron clouds of the two ions. The collision time is fast ($\approx 10^{-17}$s) relative to the dissociation time (it takes at least $\approx 10^{-14}$ s for the distance between the C and O ions to expand to twice the equilibrium bond length). Therefore the assumption of a vertical transition is valid. It should be noted, of course, that electron-electron interaction and exchange can cause the real potential to deviate considerably from a point-charge Coulomb potential, especially for low charge states. The electrostatic lens program SIMION [24] was employed to calculate the maximum (180° initial trajectory) and minimum (0° initial trajectory) flight times for ions having kinetic energies derived from the point-charge Coulomb potential,

$$E(C^q1)=7.29q_1q_2 \text{ eV} , \quad E(O^q2)=5.48q_1q_2 \text{ eV} .$$

The limiting time differences calculated for the various charge division pairs are shown by the vertical lines below the labels in Figs. 6 and 7. It is apparent that this procedure approximates the widths of the time-difference distributions reasonably well; however, because it does not take into account the kinetic-energy dependence of the efficiency, the agreement is somewhat fortuitous.

The time-difference distributions for the ion pairs arising from real dissociation events all display basically the same double-peaked structure with sharp cutoffs on the left and right sides. These cutoffs are caused by the rapid decrease in solid angle for dissociation events approaching the limiting trajectories of 0° and 180°. The valleys near the centers of the time-difference distributions, on the other hand, are caused by the restricted ranges of acceptance angles imposed by the ion kinetic energies and the exit collimator. The net effect of this is to partially separate the time-difference distributions into two components: the left-hand component containing events for which the initial trajectories of the first-arrival ions are in the upward direction and the right-hand component containing events for which they are in the downward direction. Low-kinetic-energy events contribute to the valley between the two components.

As the charge of the first-arrival ion increases, more cases contribute to the time-difference spectrum and the time-difference distributions move toward the left end of the spectrum. Eventually the left-hand component of the highest charged ion pair moves below the experimental time cutoff ($O^{3+}+C^{2+}$ and $C^{4+}+O^{4+}$) and the distributions for other ion pairs begin to overlap ($C^{4+}+O^{3+}$ with $C^{4+}+O^{4+}$).

The time-difference spectrum associated with the O^+ window is shown in the top segment of Fig. 7 to demonstrate that most of the O^+ events are generated by double collisions, as discussed in Sec. III A. Some of the O^+ events, however, are correlated with the sharp spike just above the lower time-difference threshold and with the structure spanning the region between 90 and 240 ns in Fig. 7. The threshold spike is present in all of the time-difference spectra and is believed to originate from an occasional malfunction of the MCP 2 constant fraction discriminator which caused it to generate two output signals per input signal. The structure between 90 and 240 ns is also present in the time-difference spectrum for the CO^+ and CO^{2+} windows. The origin of the TAC 2 signals that produced these coincidences is not known, but their contribution is negligible.

IV. ANALYSIS AND RESULTS

A. Simulation of time-difference distributions

Transformation of the time-difference distributions into kinetic energy distributions requires the ability to accurately calculate ion trajectories inside the gas cell and through the TOF spectrometer. The electrostatic-lens program SIMION [24] was employed for this purpose along with a Monte Carlo procedure to simulate time-difference distributions for any desired values of total-kinetic-energy release. The starting coordinates of the two ion trajectories within the beam cylinder (i.e., the center of mass of the molecule) were specified by the distance from the beam axis ρ, the distance from the TOF symmetry axis along the beam axis Y_c, and the angle with respect to the YZ plane γ, as shown in Fig. 8. The initial ion trajectories were specified by the angles θ and φ. These five coordinates were generated using a uniform distribution of random numbers ranging from 0 to 1. All values of Y_c, γ, and φ are equally probable, but ρ and θ are distributed according to the probability functions

$$P(\rho)=2\rho B^{-2} , \tag{1}$$

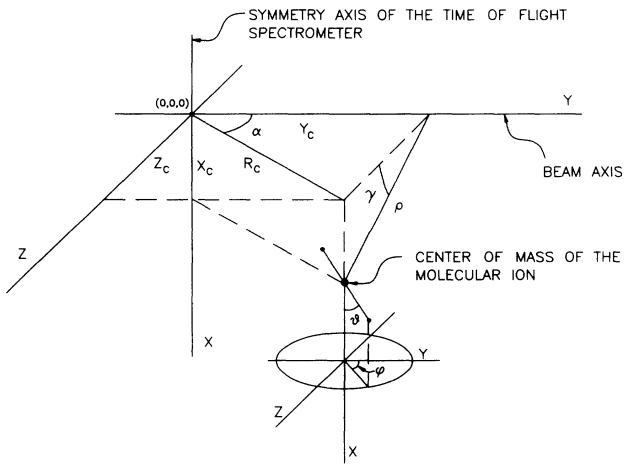

FIG. 8. Coordinate system for the Monte Carlo time-difference calculations.

$$P(\theta)=\tfrac{1}{2}\sin\theta \ , \tag{2}$$

where B is the radius of the beam cylinder. To generate a probability distribution $P(x)$ using a uniform distribution of random numbers R, the following relationship was employed:

$$R=\int_{x_{\min}}^{x} P(y)dy \ . \tag{3}$$

Applying the above relationship to the probability functions (1) and (2) gives

$$\rho=(RB^2)^{-1/2} \ , \tag{4}$$

$$\theta=\cos^{-1}(1-R) \ . \tag{5}$$

The calculational procedure was as follows. Upon picking a set of starting coordinates, the distance to the flight tube was divided into 0.1-mm intervals and the program calculated the initial X, Y, and Z velocity components. Then using the electrostatic potential array provided by SIMION, the new velocity components for the next distance interval and the flight time over the first distance interval were computed. Summing the flight times for each of the distance intervals from the starting point to MCP 2 gave the total flight time of the ion. By following this procedure for both ions of each ion pair, the distribution of time differences for the various contributing sets of trajectories (i.e., those that made it through the collimator and all the way to MCP 2) was obtained. In addition, the spectrometer transmission efficiency was directly calculated by dividing the number of "successful" ion-pair events by the number of ion-pair events attempted.

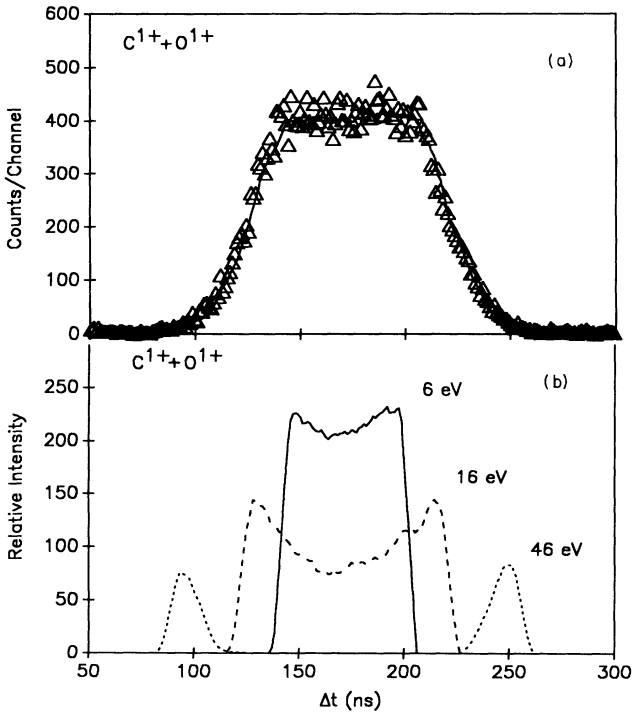

FIG. 9. (a) Experimental time-difference distribution for the dissociation reaction $CO^{2+}\rightarrow C^{+}+O^{+}$, and (b) simulated time-difference distributions for single total kinetic energies of 6, 16, and 46 eV.

In Fig. 9, the experimental time-difference distribution (a) for the case of $CO^{2+}\rightarrow C^{+}+O^{+}$ is compared with simulated time-difference distributions (b) calculated assuming three different values of total-kinetic-energy release. The simulated time-difference distributions are all normalized to the same number of attempted events, causing their relative yields to be directly proportional to the average transmission efficiencies. It is evident from Fig. 9(b) that (a) the time separation between the C^{+}-up–O^{+}-down pairs (on the low Δt side) and the C^{+}-down–O^{+}-up pairs (on the high Δt side) increases rapidly with total kinetic energy, and (b) the average transmission efficiency decreases rapidly with increasing total kinetic energy.

B. Time-to-energy transformation

Employing the above time-distribution simulation technique, response matrices were constructed for all the dissociation reactions having sufficient statistics for a meaningful analysis. Each response matrix consisted of an array of time-difference distributions in energy intervals which varied from 0.45 to 4.39 eV, depending on the range of the kinetic energies required. A schematic representation of the response matrix for the case of $CO^{2+}\rightarrow C^{1+}+O^{+}$ is shown in Fig. 10. As in the case of the time-difference distributions shown in Fig. 9(b), the relative yield of each time-difference distribution in the response matrix was proportional to the average transmission efficiency for its total kinetic energy.

Since a time-difference distribution (vector T) is related to the corresponding total kinetic-energy distribution (vector E) through the response matrix R via the matrix equation

$$T=RE \ , \tag{6}$$

the simplest approach to transforming T into E is to find the inverse of R, such that

$$E=R^{-1}T \ . \tag{7}$$

Unfortunately, as is discussed in Ref. [25], a number of technical problems having to do with the singular nature of R and the statistical uncertainties in T prevent one from obtaining meaningful kinetic-energy distributions in this way. Instead, an iterative technique described by Scofield [25,26] was used to solve this problem.

The iterative process begins by calculating a zeroth-order estimate of the kinetic-energy distribution as follows:

$$E^{(0)}=D^{(0)}(R'T) \ , \tag{8}$$

where R' is the transpose of R and $D^{(0)}=I$ (the identity matrix). Then the vector $(R'T)^{(0)}$ is obtained from the relationship

$$(R'T)^{(0)}=(R'T)E^{(0)} \tag{9}$$

and used to compute the elements of $D^{(1)}$:

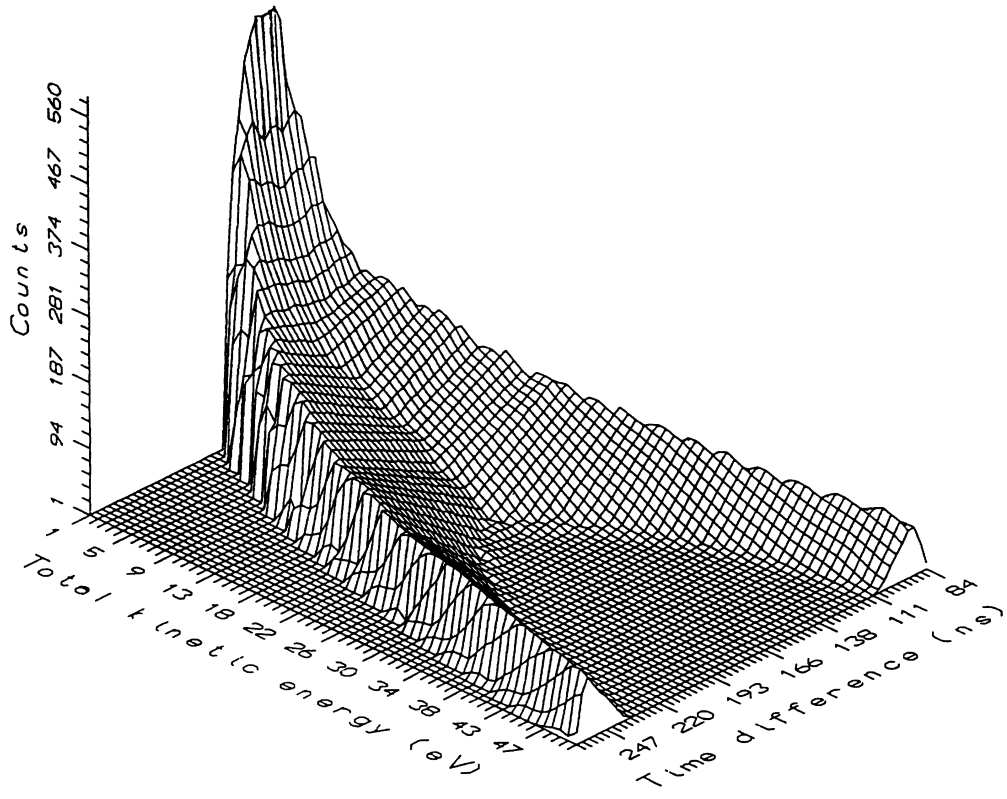

FIG. 10. Schematic representation of the response matrix for the dissociation reaction $CO^{2+} \rightarrow C^+ + O^+$.

$$D_{kl}^{(1)} = E_k^{(0)} / (R'T)_l^{(0)} \delta_{kl} \ . \tag{10}$$

After i iterations,

$$(R'T)^{(i-1)} = (R'R) E^{(i-1)} \ , \tag{11}$$

$$D_{kl}^{(i)} = E_k^{(i-1)} / (R'T)_l^{(i-1)} \delta_{kl} \ , \tag{12}$$

$$E^{(i)} = D^{(i)} (R'T) \ . \tag{13}$$

After each iteration, the new energy distribution was transformed back into a time distribution

$$T_c^{(i)} = R E^{(i)} \tag{14}$$

and compared with the experimental time distribution T. The iterative process was terminated when the reduced χ^2 value reached its minimum value (generally less than 1.5).

The above transformation method was tested by using a variety of assumed kinetic-energy distributions to construct the corresponding time-difference distributions by means of the Monte Carlo TOF program described in Sec. IV A. These time-difference distributions were then transformed back into kinetic-energy distributions via the Scofield iterative technique and the resulting distributions compared with the original ones. In general, the main features of the original energy distributions were faithfully reproduced in both overall shape and average energy position. However, the energy distributions obtained from the Scofield iteration process had a tendency to display additional minor structural features (e.g., wiggles and bumps) that were not present in the original energy distributions. Also, these tests indicated that the method is not capable of resolving features that are less than about 5 eV apart, no matter how narrow they are.

The kinetic energy distribution obtained from the time-distribution for $CO^{2+} \rightarrow C^+ + O^+$ via the Scofield iterative method is shown by the solid curve in Fig. 11(a). As an additional check on the reliability of the method, this kinetic-energy distribution was also extracted using a least-squares fitting technique similar to the one employed by Saito and Suzuki [27] and by Lablanquie *et al.* [2]. The fitting functions for this procedure were the same ones used to construct the response matrix employed in the Scofield method. The kinetic-energy distribution obtained from the least-squares fit is shown by the dashed curve in Fig. 11(a). The agreement between the two methods is excellent. The Scofield iterative method was found to require much less computer time than the least-square fitting procedure, and therefore it was used to analyze all the other time-difference distributions.

In Fig. 11(b), the $C^+ + O^+$ kinetic-energy distribution obtained in the present work is compared with the one obtained by Lablanquie *et al.* [2] using 110-eV photons. Both distributions have been normalized to the same area. Overall, the structural features are quite similar with distinct components appearing around 4, 11 and 20 eV. The present energy distribution for excitation by Ar ions exhibits much more intensity in the 20-eV com-

ponent relative to the 11-eV component than the energy distribution for photoionization and it displays an additional high-energy component centered around 40 eV.

Kinetic-energy distributions for all of the time-distributions analyzed are compared in Fig. 12. These curves are normalized to unity at their maximum intensity points. Because of the limited resolution and statistics of the experiments, minor structural features in these distributions probably should not be taken seriously. In particular, as can be deduced from Figs. 6 and 7, the kinetic-energy distributions shown for $CO^{4+} \rightarrow C^{3+} + O^{+}$, $CO^{6+} \rightarrow C^{4+} + O^{2+}$, and $CO^{7+} \rightarrow C^{4+} + O^{3+}$ are obviously subject to relatively large errors because of the poor statistics.

As a means of estimating the statistical reliability of the kinetic-energy distributions, the statistical errors were used to randomly modify the shapes of the time-difference distributions. This was accomplished by using a random number generator to add to or subtract from each data point a number of counts ranging from zero up to the statistical error. The modified time-difference distributions were then transformed to total-kinetic-energy distributions. Surprisingly, in all cases they differed only slightly from the total-kinetic-energy distributions obtained from the original data.

The average total kinetic energies and widths of the kinetic-energy distributions at their half maximum points are listed in Table I. The errors assigned to the average total kinetic energies took into account (a) the statistical uncertainties of the time-difference distribution using the procedure described above, (b) the estimated uncertainty associated with the time-distribution simulation procedure, and (c) differences between the final "calculated" time-difference distribution and the measured distribution.

TABLE I. Average values and widths of the total-kinetic-energy distributions.

Parent molecular ion	Product ion pair	E_{av} (eV)	FWHM (eV)
CO^{2+}	$C^{+}+O^{+}$	20±1	20
CO^{3+}	$C^{2+}+O^{+}$	37±3	43
	$C^{+}+O^{2+}$	43±5	50
CO^{4+}	$C^{3+}+O^{+}$	65±5	70
	$C^{2+}+O^{2+}$	68±6	57
CO^{5+}	$C^{3+}+O^{2+}$	105±10	79
	$C^{2+}+O^{3+}$	132±12	97
CO^{6+}	$C^{4+}+O^{2+}$	127±12	128
	$C^{3+}+O^{3+}$	162±17	80
CO^{7+}	$C^{4+}+O^{3+}$	162±21	161

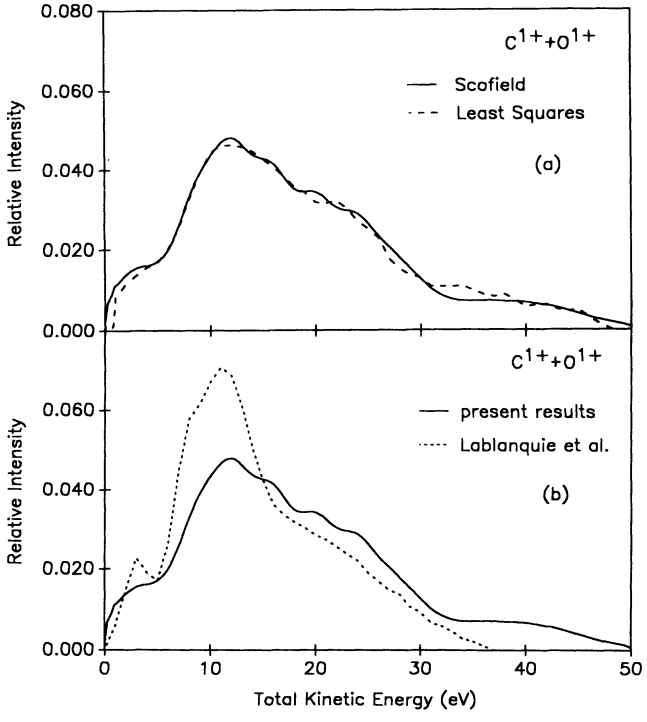

FIG. 11. (a) Comparison of the $C^{+}+O^{+}$ total-kinetic-energy distribution obtained in the present work by the Scofield iterative method (solid line) and a least-squares fitting procedure (dashed line). (b) Comparison of the $C^{+}+O^{+}$ total-kinetic-energy distribution obtained in the present work with that obtained by Lablanquie *et al.* [2].

V. DISCUSSION

A detailed analysis of the total-kinetic-energy distribution resulting from the production of CO^{2+} by photoionization and its subsequent dissociation into C^{+} and O^{+} has been carried out by Lablanquie *et al.* [2]. These investigators also performed *ab initio* calculations to obtain the potential energy curves for the electronic states of CO^{2+} lying between 35 and 60 eV. To aid in the following discussion, the potential-energy curves for the first few states of CO^{2+} are shown in Fig. 13. These curves were reproduced from Fig. 9 of Ref. [2]. Lablanquie *et al.* deconvoluted their total-kinetic-energy distribution into six components having energies of 1.8, 3.6, 7.9, 11.6, 15.6, and 22.5 eV. By adding to these kinetic energies, the dissociation energy of CO (11.11 eV), the ionization energy of C (11.26 eV), the ionization energy of O (13.61 eV), and, in the case of the $C^{+}(^{2}P)+O^{+}(^{2}D)$ asymptotic limit, the $O^{+}(^{2}D)$ excitation energy (3.32 eV), the corresponding CO^{2+} excitation energies were determined. Based on a comparison of these excitation energies with the potential-energy diagram for CO^{2+} (see Fig. 13), Lablanquie *et al.* assigned the 3.6-eV component to the $^{3}\Pi$ ground state and the 7.9-eV component to the $^{3}\Sigma^{-}$ state. At excitation energies corresponding to the 11.6-eV component (47.6 eV), the density of states becomes so high that population of single, well-resolved states is no longer possible.

Comparison of the energy distribution obtained in the present work for the dissociation of CO^{2+} with that of Lablanquie *et al.* [see Fig. 11(b)] indicates that the same low-lying states are populated in 97-MeV Ar-ion collisions. However, it is evident that, on average, substan-

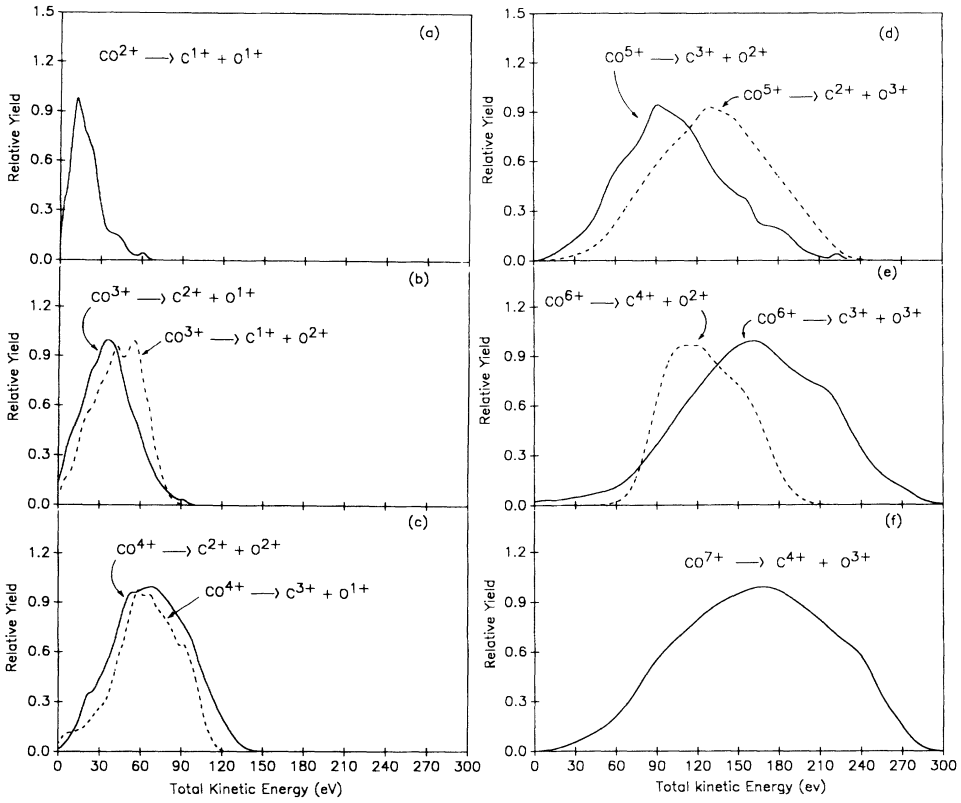

FIG. 12. Total-kinetic-energy distributions for all the prominent dissociation channels observed for CO^{2+} through CO^{7+}.

tially higher excitation energies are produced by Ar-ion collision-induced ionization than by photoionization. The average total kinetic energy obtained from the present measurements is 20 eV, which corresponds to a CO^{2+} excitation energy around 56 eV, while the average total kinetic energy for photoionization is 14.5 eV. The point-charge Coulomb potential energy [relative to the $C^+(^2P)+O^+(^4S)$ asymptotic state] is shown by the dotted curve in Fig. 13. The total kinetic energy corresponding to the point-charge Coulomb potential at the center of the Franck-Condon zone is 12.8 eV, which is considerably lower than the average total kinetic energy observed in the present experiment.

Although Lablanquie *et al.* did not perform a detailed analysis of the kinetic-energy distribution for $CO^{3+} \rightarrow C^{2+}+O^+$, they did observe two components

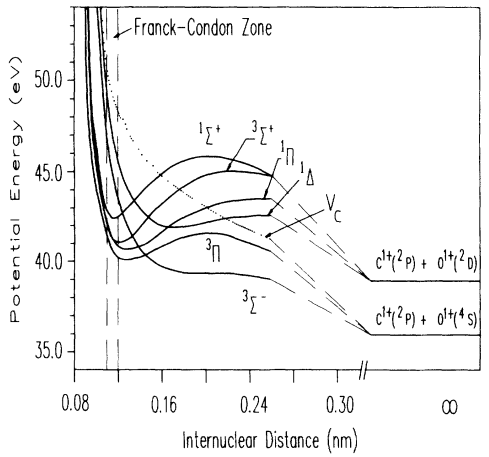

FIG. 13. Potential-energy curves for the low-energy states of CO^{2+}, reproduced from Fig. 9 of Ref. [2]. The dotted curve shows the point-charge Coulomb potential.

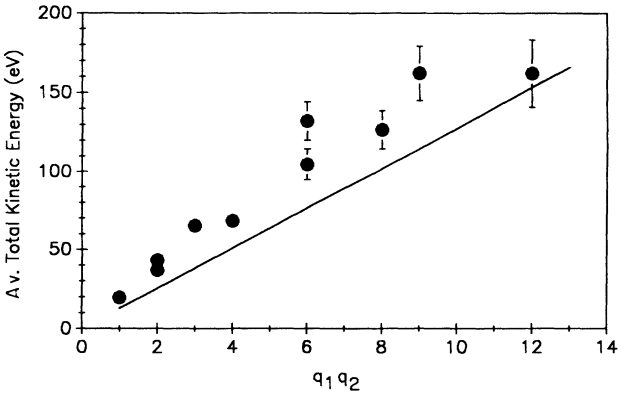

FIG. 14. Comparison of the average total kinetic energy for different q_1+q_2 charge pairs (data points) with the total kinetic energy predicted by the point-charge model (solid line).

with estimated energies of 20 and 30 eV. They were unable to see the other dissociation pathway leading to $C^+ + O^{2+}$ product ions because its time-difference distribution was obscured by that for the $C^+ + O^+$ ion pair since they did not utilize two parameter data acquisition. The total-kinetic-energy distribution obtained in the present work for the $C^{2+} + O^+$ ion pair peaks around 40 eV and shows only weak indications of possible structure in the vicinity of 10 and 25 eV. The average total kinetic energy observed for this case (37 eV) is evidently quite a bit higher than that produced by photoionization.

Potential-energy curves for CO molecular ions having charges greater than 2 have not yet been calculated. Even so, it is clear from the curves calculated for CO^{2+} by Lablanquie *et al.* that the density of states increases rapidly with charge state. Hence it is not surprising that the total-kinetic-energy distributions obtained in the present work for the dissociation of CO molecular ions having charges of 3+ or greater are rather featureless (see Fig. 12). The rapid increase in the widths of the kinetic-energy distributions indicates that the potential-energy curves become more repulsive in the region of the Franck-Condon zone (i.e., they rise more steeply) as electrons are removed from the CO molecule. In this context, it is interesting to compare the average total kinetic energies with those corresponding to a point-charge Coulomb potential. Such a comparison is shown in Fig. 14. It is evident that all of the average total kinetic energies obtained in the present measurements exceed those calculated using the simple point-charge model. This same trend has been observed in Coulomb explosion experiments with 4.0- and 8.4-MeV CO^{2+} ions [28]. By referring back to Fig. 13, it may be seen that the potential-energy curves for the low-energy states CO^{2+} lie somewhat below the point-charge Coulomb potential. Hartung *et al.* [29] found this to be the case for highly charge N_2 molecular ions ($q = +7$, $+8$, and $+9$) as well. These investigators performed self-consistent field calculations of the statistical average potential-energy curves connecting to a number of asymptotic orbital configurations. The average total kinetic energy released in forming two N^{4+} ions in their ground states was found to be 16.2 eV less than that given by the point-charge model. For highly excited N^{4+} ion configurations with a K vacancy in both ions, however, average total kinetic energy releases ranging up to 18 eV above the point-charge model prediction were obtained.

The average excitation energy of the parent molecular ion can be estimated using the average total kinetic energies (Table I) and the separated atom ionization energies. This procedure, of course, assumes the dissociation product ions are left in their ground states. Estimates of the average excitation energies are presented in Table II, along with the energies of the corresponding (ground-state) asymptotic limits. It may be seen from this table that in all cases where two dissociation pathways were observed, except for the CO^{6+} case, the pathway leading to the lower-energy asymptotic limit has the lower average excitation energy. Another noteworthy feature of the average excitation energies is that they increase linearly with the number of electrons removed from the CO molecule. The slope of this linear relationship is 78 eV/electron for charges of 3+ and above.

TABLE II. Estimated average excitation energies for CO molecular ions produced in 96-MeV Ar^{14+}-ion collisions.

Molecular ion	Product ion pair	Average excitation energy (eV)	Lowest asymptotic limit (eV)
CO^{2+}	$C^+ + O^+$	56	36.1
CO^{3+}	$C^{2+} + O^+$	97	60.4
	$C^+ + O^{2+}$	114	71.2
CO^{4+}	$C^{3+} + O^+$	173	108.3
	$C^{2+} + O^{2+}$	164	95.5
CO^{5+}	$C^{3+} + O^{2+}$	248	143.4
	$C^{2+} + O^{3+}$	283	150.4
CO^{6+}	$C^{4+} + O^{2+}$	334	207.9
	$C^{3+} + O^{3+}$	360	198.3
CO^{7+}	$C^{4+} + O^{3+}$	425	262.8

VI. CONCLUSIONS

Ion-ion coincidence time-of-flight spectroscopy has been used to study the total kinetic energy released in the dissociation of multicharged CO molecular ions produced in collisions with 97-MeV Ar^{14+} ions. Time-difference distributions were obtained for all the prominent dissociation channels of CO^{2+} through CO^{7+}. An iterative matrix transformation procedure was used to convert the time-difference distributions into total-kinetic-energy distributions.

Comparison of the present total-kinetic-energy distributions for CO^{2+} and CO^{3+} with the results of Lablanquie *et al.* [2] indicated that Ar-ion-impact ionization forms molecular ions in higher states of excitation, on average, than photoionization. The average excitation energy produced in Ar-ion collisions increases by approximately 78 eV per electron removed from the molecule for charge states of 3+ and above.

The finding that the average total kinetic energy released in the dissociation of molecular ions produced by Ar-ion impact is systematically greater than that predicted by the simple point-charge model is somewhat puzzling. The few theoretical results that are currently available concerning potential-energy curves for multicharged molecular ions tend to indicate that, in the Franck-Condon zone, the point-charge Coulomb potential lies above most of the states which connect to low-energy asymptotic configurations. Therefore this observation may indicate that most of the dissociation channels populated in Ar-ion collisions lead to highly excited product ions.

Experiments of the type described here may be capable of extending the investigation of highly charged molecular ions to even higher charge states by focusing on collision events in which the projectile captures one or more electrons. Electron capture collisions occur at much smaller impact parameters, on average, than collisions in which the projectile charge remains unchanged. This, in turn, leads to the production of more highly charged

recoil ions. Maurer [16], for example, found that the highest-charged ion observable in 40-MeV Ar^{13+} collisions with O_2 increased from O^{4+} for projectile charge-unchanged collisions to O^{5+} for one-electron capture collisions to O^{7+} for two-electron capture collisions.

Note added in proof. Potential-energy curves of low-lying electronic states in CO^{2+} and CO^{+} computed using all-electron *ab initio* molecular-orbital methods have just been published by Krishnamurthi *et al.* [30]. Significant differences in the shapes and ordering of the potential-energy curves exist between these results and those of Lablanquie *et al.* [2].

ACKNOWLEDGMENTS

This work was sponsored by the U. S. Department of Energy, Division of Chemical Sciences, and the Robert A. Welch Foundation.

*Present address: Weizmann Institute, Rehovot 76100, Israel.

†On leave from the Department of Physics, Faculty of Science and Mathematics, University of Zagreb, Croatia, Yugoslavia.

‡Present address: Institut Curie, 11 rue Pierre et Marie Curie, 75231 Paris CEDEX 05, France.

[1] A. P. Hitchcock, P. Lablanquie, P. Morin, E. Lizon, A. Lugrin, M. Simon, P. Thirty, and I. Nenner, Phys. Rev. A **37**, 2448 (1988).

[2] P. Lablanquie, J. Delwiche, M.-J. Hubin-Franskin, I. Nenner, P. Morin, K. Ito, J. H. D. Eland, J.-M. Robbe, G. Gandara, J. Fournier, and P. G. Fournier, Phys. Rev. A **40**, 5673 (1989).

[3] F. H. Dorman and J. D. Morrison, J. Chem. Phys. **35**, 575 (1961).

[4] S. E. Kupriyanov, Zh. Tekh. Fiz. **34**, 861 (1964); [Sov. Phys.—Tech. Phys. **9**, 659 (1964)].

[5] A. S. Newton and A. F. Sciamanna, J. Chem. Phys. **53**, 132 (1970).

[6] J. H. Beynon, R. M. Caprioli, and J. W. Richardson, J. Am. Chem. Soc. **93**, 1852 (1971).

[7] G. R. Wright, M. J. van der Wiel, and C. E. Brion, J. Phys. B **9**, 675 (1976).

[8] B. Brehm and G. De Frenes, Int. J. Mass Spectom. Ion Phys. **26**, 251 (1978).

[9] T. Masuoka and J. A. R. Samson, J. Chem. Phys. **80**, 1093 (1981).

[10] J. M. Curtis and R. K. Boyd, J. Chem. Phys. **80**, 1150 (1984).

[11] T. Masuoka, J. Chem. Phys. **82**, 3921 (1985).

[12] C. L. Cocke, Phys. Rev. A **20**, 749 (1979).

[13] H. Tawara, T. Tonuma, H. Shibata, M. Kase, T. Kambara, S. H. Be, H. Kumagai, and I. Kohno, Phys. Rev. A **33**, 1385 (1986).

[14] R. J. Maurer, C. Can, and R. L. Watson, Nucl. Instrum. Methods B **27**, 512 (1987).

[15] H. Tawara, K. Baba, T. Matsuo, M. Kase, T. Kambara, H. Kumagai, and I. Kohno, Nucl. Instrum. Methods B **23**, 203 (1987).

[16] R. J. Maurer, Ph.D. dissertation, Texas A&M University, 1988.

[17] G. Sampoll, O. Heber, R. J. Maurer, P. A. Scott, and R. L. Watson, Nucl. Instrum. Methods B **40**, 308 (1989).

[18] K. Wohrer, G. Sampoll, R. L. Watson, M. Chabot, O. Heber, and V. Horvat (unpublished).

[19] R. L. Watson and R. J. Maurer, Nucl. Instrum. Methods A **262**, 99 (1987).

[20] W. C. Wiley and I. H. McLaren, Rev. Sci. Instrum. **26**, 1150 (1955).

[21] See, for example, G. Dujardin, S. Leach, O. Dutuit, P.-M. Guyon, and M. Richard-Viard, Chem. Phys. **88**, 339 (1984); D. M. Curtis and J. H. D. Eland, Int. J. Mass. Spectom. Ion Phys. **63**, 241 (1985), and references therein.

[22] J. C. Levin, R. T. Short, C.-S. O, H. Cederquist, S. B. Elston, J. P. Gibbons, I. A. Sellin, and H. Schmidt-Bocking, Phys. Rev. A **36**, 1694 (1987).

[23] O. Heber, R. L. Watson, and G. Sampoll, Nucl. Instrum. Methods B **56**, 232 (1991).

[24] D. A. Dahl and J. E. Delmore, Idaho National Engineering Laboratory Report No. EGG-CD-7233 Rev. 1, 1987 (unpublished).

[25.] J. E. Monahan, in *Scintillation Spectroscopy of Gamma Radiation,* edited by S. M. Shafroth (Gordon and Breach, New York, 1967).

[26] N. E. Scofield, U. S. Naval Defense Laboratory Report No. TN-477, 1960 (unpublished).

[27] N. Saito and H. Suzuki, Chem. Phys. Lett. **129**, 419 (1986).

[28] Daniel Zajfman (private communication).

[29] H. Hartung, B. Fricke, T. Morovic, W. -D. Sepp, and A. Rosen, Phys. Lett. **69A**, 87 (1978).

[30] V. Krishnamurthi, K. Nagesha, V. R. Marathe, and D. Mathur, Phys. Rev. A **44**, 5460 (1991).